Model of a truncated fast rotating flow at infinite Reynolds number

L. Bourouiba[a)]

McGill University, 805 Sherbrooke W., Room 945, Montréal, Québec H3A 2K6, Canada

The purpose of this study is to examine the strongly rotating limit of a turbulent flow theoretically and numerically. The goal is to verify the predictions of asymptotic theories. Given the limitations of experimental and dissipative numerical approaches to this problem, we use classical equilibrium statistical mechanics. We apply the statistical mechanics approach to the inviscid truncated model of strongly rotating turbulence (in the *small Rossby* number range) and derive the theoretical spectra of the decoupled model. We use numerical simulations to complement these derivations and examine the relaxation to equilibrium of the inviscid unforced truncated rotating turbulent system for different sets of initial conditions. We separate our discussion into two time domains: the discussion of the decoupled phase with time below a threshold time $t_\star$, for which a new set of invariants S are identified, and the coupled phase with a time beyond $t_\star$, for which the quantities S are no longer invariants. We obtain a numerical evaluation of $t_\star$ which is coherent with the theoretical asymptotic expansions. We examine if the quantities S play a constraining role on the coupled dynamics beyond $t > t_\star$. We find that the theoretical statistical predictions in the decoupled phase capture the horizontal dynamics of the flow. In the coupled phase, the invariants S are found to still play a constraining role on the short-timescale horizontal dynamics of the flow. These results are discussed in the larger context of previous rotating turbulence studies. © *2008 American Institute of Physics.*
[DOI: 10.1063/1.2958319]

I. INTRODUCTION

Rotation plays an important role on the dynamics of large scale geophysical and astrophysical flows. The Coriolis force appears only in the linear part of the momentum equations, but if strong enough, can radically change the dynamics. The strength of the applied rotation, Ω, only has an appreciable influence when it is comparable or larger than the nonlinear term. The nondimensional Rossby number Ro is a measure of the strength of the rotation. When $\Omega \to \infty$, Ro $\to 0$. When the Coriolis force is applied, inertial waves are solutions of the linear momentum equations. Their frequencies vary from zero to 2Ω.[1] The zero linear frequency modes correspond to two-dimensional (2D) structures, aligned with the rotation axis. In the full nonlinear problem, the large range of frequencies of the inertial waves is at the origin of a complex nonlinear interplay of interactions involving the 2D structures and the wave [three-dimensional (3D)] modes.

Rotating turbulence has been studied by using various approaches. Experimental studies[2–7] and numerical simulations of forced[8–10] and decaying[11,12] rotating turbulence have been performed. Three distinct rotation regimes were identified for decaying rotating turbulent flows:[13] the *weakly rotating* range, the *intermediate* Ro range, and the *small* Ro range. The intermediate range was characterized by a mechanism of maximum leakage of energy from 3D (wave) modes toward 2D zero-frequency modes and an asymmetry of the vorticity distribution. The small Ro range was characterized

by a minimal energy transfer between zero-frequency modes and wave (3D) modes, an upscale transfer of energy for the zero-frequency modes, and no significant vorticity distribution asymmetry. *A posteriori*, most results of experimental and numerical studies cited above that observe an increase in the maximum vorticity asymmetry and dominant 2D mode growth fall into the intermediate Ro range. The mechanisms causing the growth of the 2D modes in this regime are still unclear. Both nonlinear effects, such as the near-resonant interactions[14] in forced numerical simulations, and linear effects[15] in decay inhomogeneous flow experiments are argued to be at the origin of the generation of columnar structures repeatedly observed in this regime.[4] More investigation is needed of the asymmetry mechanisms typical of this intermediate Ro regime and the timescales of the mechanisms involved.

All of the above approaches (experimental, forced, and decay numerical simulations in homogeneous and inhomogeneous rotating turbulence) can be used to pursue the understanding of the intermediate Ro regime. This is not the case for the small Ro regime. The tools available to study the small Ro regime are less obvious. An attempt using a statistical approach and quasinormal Markovian approximations was used[16] and focused on the dynamics of the resonant interactions. However, this study only captures the dynamics of the 3D wave modes and the effects of the pure resonant interactions, which are not the only interactions present for asymptotically small but nonzero Ro numbers. Using an experimental approach to study this extreme regime is difficult due to the strength of rotation rates needed. In addition, there is difficulty in interpreting the experimental results when other effects are involved (e.g., Ekman layer dynamics or

a)Electronic mail: lydia.bourouiba@mail.mcgill.ca.

20, 075112-1   © 2008 American Institute of Physics

inhomogeneity of the flow). Direct numerical simulations of both forced and decaying rotating turbulences in the strong rotation limit have the advantage with regards to these constraints. However, they also have limitations. When performing forced and decay simulations of the small Ro regime, like for all other rotating regimes, a sufficient resolution of the inertial range is needed in order to limit the effect of the dissipation range on the scales of interest. In the small Ro regime, this need for a sufficiently large inertial range, combined with (1) a typically slow nonlinear timescale that imposes a long numerical integration time in order to analyze the long-timescale dynamics and (2) a large amplitude for the Coriolis force which imposes a small timestep needed for the numerical integration, leads to major numerical limitations.

Due to the limitations of both forced and decaying simulations, we choose to focus this study of the small Ro regime on the statistical equilibrium and inviscid dynamics of its truncated governing equations. The inviscid approach takes root in equilibrium statistical mechanics, which is our primary theoretical tool. In addition, we use complementary numerical simulations of the inviscid spectrally truncated equations of the rotating flow. This approach has the advantage of allowing a smaller resolution and thus a much longer integration time. A sufficiently long integration time is critical for the better understanding of the small Ro regime. The study of inviscid flows with the method of equilibrium statistical mechanics is a theoretical approach to an idealized problem. However, this theoretical approach has proven helpful in understanding numerous fundamental turbulence problems. In fact, the use of equilibrium statistical mechanics theory for the study of inviscid flows captured the inverse energy cascade of 2D turbulence and the forward energy cascade of isotropic turbulence.[17–19] The inviscid flow is expected to relax to absolute equilibrium. For a review of the statistical theories and equilibrium spectra see Ref. 20, and for a complete exposé of the latest statistical theories for geophysical flows see Ref. 21.

In addition, the numerical study of truncated inviscid flow models has been used to investigate the relaxation to equilibrium for 2D turbulence[22] and provided a general agreement with equilibrium statistical theory. Statistical equilibria of other sets of truncated equations were also investigated: quasigeostrophic flows,[21,23,24] weak turbulence flows for shallow water equations,[25] the nonhydrostatic rotating Boussinesq equations,[26] 2D turbulence shear flow,[27] and stratified flows.[28] The relaxation to equilibrium of a spectrally truncated 3D isotropic flow was also recently studied numerically.[29,30] Finally, spectrally truncated 3D rotating turbulence was studied numerically by Yamazaki *et al.* They examined moderate rotation rates and observed a relaxation to isotropic equipartition. They also observed that rotation introduced a delay and scale dependency on the relaxation-to-equilibrium timescale. The fundamental difference among the inviscid truncated systems listed above is the number and properties of their physical invariants. These invariants, or conserved quantities, play a key role in both the formalism of the inviscid statistical equilibrium and the understanding of the dissipative dynamical counterpart.

In this study, we apply the equilibrium statistical mechanics approach to truncated inviscid flows subject to a strong rotation. The model of equations predicted by the singular perturbations in this regime conserves a new set of invariants. Using this new set of invariants, we first derive the predicted equilibrium spectra associated with the new invariant quantities. We then turn to numerical simulations to compare the theoretical spectra obtained to the numerical inviscid truncated solutions. We thus intend to examine four primary questions: (1) Does the theoretical model of decoupled equations derived based on the assumptions of the asymptotic expansions capture the dynamics of the spectrally truncated solutions? (2) If this is not the case, are some features of the small Ro regime nevertheless captured? (3) If this is the case, on what timescale does this hold, and is that time consistent with the timescale predicted by the asymptotic theories? (4) How do the dynamics change beyond this threshold time and are the invariants still playing a constraining role?

In Sec. II, the problem and equations of rotating turbulence are introduced and the timescales of the problems are discussed. In Sec. III, we apply the method of equilibrium statistical mechanics to the rotating turbulence problem and discuss its new invariants. We also derive their associated statistical equilibrium spectra. The theoretical spectra are then compared to the numerical solutions of the truncated inviscid equations in Sec. IV. We further discuss our approach and the results in Sec. V.

II. EQUATIONS AND ROTATING TURBULENCE THEORIES

A. Full equations

In a rotating frame of reference, the incompressible inviscid nondimensional momentum equation is

$$\frac{\partial \mathbf{u}}{\partial t} + \mathrm{Ro}(\mathbf{u} \cdot \nabla)\mathbf{u} + \hat{\mathbf{z}} \times \mathbf{u} = -\nabla p, \quad \nabla \cdot \mathbf{u} = 0, \tag{1}$$

where $\mathrm{Ro} = U/2\Omega L$ is the Rossby number, a dimensionless measure of the relative size of the advection and rotation terms, $\boldsymbol{\Omega} = \Omega\hat{\mathbf{z}}$ is the rotation vector, $f = 2\Omega$, $\mathbf{u} = (u, v, w)$ is the velocity vector, and p is the reduced pressure that includes the centrifugal term. Without loss of generality, the rotation axis has been chosen to be in the vertical direction $\hat{\mathbf{z}}$. Nondimensionalization was done using $(2\Omega)^{-1}$, L, and U as characteristic time, length, and velocity, respectively. When linearized about a rest state, the normal modes $\mathbf{n}_{\lambda_s}$, with the eigenvalues $\lambda_s = sfk_z/k$ and $s = \pm$ can be derived (see Appendix for details). This new basis can be used to re-express the implicitly nondivergent velocity field as

$$\mathbf{u}(\mathbf{r}) = \sum_{\mathbf{k}} \mathbf{u}(\mathbf{k})\exp(i\mathbf{k} \cdot \mathbf{r})$$

$$= \sum_{\mathbf{k}} [A_+(\mathbf{k}, t)\mathbf{n}_+(\mathbf{k}) + A_-(\mathbf{k}, t)\mathbf{n}_-(\mathbf{k})]\exp(i\mathbf{k} \cdot \mathbf{r}), \tag{2}$$

with $A_s(\mathbf{k}, t) = a_s(\mathbf{k})\exp(i\lambda_s t)$. The reality condition [$\mathbf{u}(\mathbf{r})$ must be real] implies that $\mathbf{u}^*(\mathbf{k}) = \mathbf{u}(-\mathbf{k})$. Thus, the Fourier components $a_s(\mathbf{k})$ satisfy $a_s^*(\mathbf{k}) = a_s(-\mathbf{k})$.

B. Two-timescale problem, resonance condition

The Ro number can also be considered as the ratio between two timescales: $Ro = T_1/T_2$, where $T_1 = (2\Omega)^{-1}$ is a rapid timescale associated with the rotation and $T_2 = L/U$ is a slow timescale associated with the nonlinear interactions.

When rotation is strong, $Ro \rightarrow 0$ and the timescale separation between T_1 and T_2 becomes larger. Thus, Eq. (1) evolves on both a slow vortical timescale that could be re-expressed as $\tau_1 = Ro\, t$ and a fast wave timescale $\tau_0 = t$, where t is the nondimensional time $t = \tilde{t} f$ and $\tilde{t}$ is the physical dimensional time. A multiple timescale asymptotic expansion can thus be performed. The leading-order part of this two-timescale problem is equivalent to the linear counterpart of Eq. (1) and has inertial wave solutions (as seen in Appendix). The nondimensional counterparts of the dimensional frequencies λ_s are $\omega_{s_{\mathbf{k}}}(\mathbf{k}) = s_{\mathbf{k}}\hat{\mathbf{z}} \cdot \mathbf{k}/|\mathbf{k}| = s_{\mathbf{k}} k_z/k = s_{\mathbf{k}} \cos(\theta_{\mathbf{k}})$, with $s_{\mathbf{k}} = \pm 1$ and $\theta_{\mathbf{k}}$ being the angle between $\mathbf{k}$ and the axis of rotation. In the following, $\omega_{s_{\mathbf{k}}}(\mathbf{k})$ is also denoted by $\omega_{s_{\mathbf{k}}}$.

At the first order of the expansion, the only interacting triads that have a significant contribution on the slow timescale τ_1 are those that satisfy the *resonance condition*[1,31]

$$\omega_{s_{\mathbf{k}}}(\mathbf{k}) + \omega_{s_{\mathbf{p}}}(\mathbf{p}) + \omega_{s_{\mathbf{q}}}(\mathbf{q}) = 0. \qquad (3)$$

In other words, the modal solutions are given by the two equations

$$\mathbf{k} + \mathbf{p} + \mathbf{q} = 0 \quad \text{and} \quad s_{\mathbf{k}}\frac{k_z}{|\mathbf{k}|} + s_{\mathbf{p}}\frac{p_z}{|\mathbf{p}|} + s_{\mathbf{q}}\frac{q_z}{|\mathbf{q}|} = 0. \qquad (4)$$

The zero-frequency modes belong to the Fourier-space plane defined by $k_z = 0$, corresponding to the vertically averaged real-space velocity field.

C. Modal decomposition

Our approach is to classify the modes into two groups: wave modes with nonzero frequencies, corresponding to $k_z \neq 0$ in Fourier space (also referred to as 3D modes), and zero-frequency modes. The following notation is used:

If $\mathbf{k} \in V_{\mathbf{k}} = \{\mathbf{k} | k \neq 0 \text{ and } k_z = 0\}$

then $\mathbf{u}(\mathbf{k}) = \mathbf{u}_{2D}(\mathbf{k}_h) + w(\mathbf{k}_h)\hat{\mathbf{z}}$,

$$\qquad (5)$$

If $\mathbf{k} \in W_{\mathbf{k}} = \{\mathbf{k} | k \neq 0 \text{ and } k_z \neq 0\}$ then $\mathbf{u}(\mathbf{k}) = \mathbf{u}_{3D}(\mathbf{k})$.

The total energy

$$E = \frac{1}{2}\sum_{\mathbf{k}} |\mathbf{u}(\mathbf{k})|^2 \qquad (6)$$

becomes

$$E = E_{2D} + E_w + E_{3D}, \qquad (7)$$

with

$$E_{2D} = \frac{1}{2}\sum_{\mathbf{k} \in V_{\mathbf{k}}} |\mathbf{u}_{2D}(\mathbf{k})|^2,$$

$$E_w = \frac{1}{2}\sum_{\mathbf{k} \in V_{\mathbf{k}}} |w(\mathbf{k})|^2, \qquad (8)$$

and

$$E_{3D} = \frac{1}{2}\sum_{\mathbf{k} \in W_{\mathbf{k}}} |\mathbf{u}(\mathbf{k})|^2,$$

which have corresponding spectra. The latter are governed by

$$\frac{\partial E_{3D}}{\partial t}(\mathbf{k} \in W_{\mathbf{k}}, t) = (T_{33\rightarrow 3} + T_{32\rightarrow 3} + T_{3w\rightarrow 3})(\mathbf{k} \in W_{\mathbf{k}}, t),$$

$$\frac{\partial E_{2D}}{\partial t}(\mathbf{k} \in V_{\mathbf{k}}, t) = (T_{22\rightarrow 2} + T_{33\rightarrow 2})(\mathbf{k} \in V_{\mathbf{k}}, t), \qquad (9)$$

$$\frac{\partial E_w}{\partial t}(\mathbf{k} \in V_{\mathbf{k}}, t) = (T_{2w\rightarrow w} + T_{33\rightarrow w})(\mathbf{k} \in V_{\mathbf{k}}, t),$$

where T is the Fourier-space energy transfer. Transfers are distinguished by the types of interactions, e.g., $33 \rightarrow 2$ stands for the interactions between two 3D wave modes that contribute to the 2D equation.

In the $Ro \rightarrow 0$ limit, it is thought that only resonant interactions make a significant contribution to the slow dynamics until a certain time at which a higher-order expansion can be continued.[32] Only a subset of 3D wavenumbers can satisfy the resonance condition in the $33 \rightarrow 3$, $32 \rightarrow 3$, and $3w \rightarrow 3$ interactions, but the $32 \rightarrow 3$ and $3w \rightarrow 3$ resonant triads do not transfer energy to the 2D and w modes, respectively. In fact, the interaction coefficient of the 2D mode in these resonant interactions was shown to be zero.[31] The transfers are thus said to be "catalytic." For example, in the $32 \rightarrow 3$ interaction, the 2D mode plays the role of a catalyzer, facilitating the nonlinear interaction and energy exchange between the two 3D modes, but without receiving or losing energy itself (the 2D mode). This last property is a key point in asymptotic theories, predicting a decoupling between the inertial waves and the 2D coherent structures in a rapidly rotating flow. Averaging the interactions between fast waves led Babin et al.[33] to obtain an equation governing the vertically averaged 2D structures of the flow decoupled from the wave dynamics in the limit of small Ro. However, Cambon et al.[34] argued later that for an unbounded domain, coupling terms between the 2D and wave modes remain active even at $Ro = 0$. That is, no decoupling was achievable.

When only resonant interactions contribute to the energy transfers, the asymptotic energy equations are

$$\frac{\partial E_{3D}}{\partial t}(\mathbf{k} \in W_\mathbf{k}, t) = T_{33\to3,\text{res}} + T_{32\to3,\text{res}} + T_{3w\to3,\text{res}},$$

$$\frac{\partial E_{2D}}{\partial t}(\mathbf{k} \in V_\mathbf{k}, t) = T_{22\to2}, \qquad (10)$$

$$\frac{\partial E_w}{\partial t}(\mathbf{k} \in V_\mathbf{k}, t) = T_{2w\to w},$$

where the subscript $\{jk\to i, \text{res}\}$ denotes resonant $jk\to i$ interactions (4). The time and wavenumber dependence in Eq. (10) has been omitted. $22\to2$ and $2w\to w$ interactions are trivially resonant, since all modes involved have zero frequency. It appears from Eq. (10) that the equation for E_{2D} is decoupled from the E_{3D} equation and is also similar to that governing the 2D turbulence. The equation for E_w is also decoupled from that of E_{3D} and takes the form of a passive tracer advected by the 2D velocity field $\mathbf{u}_{2D}$. On the other hand, the E_{3D} remains affected by the $k_z=0$ dynamics through the set of catalytic resonant triads $32\to3$ and $3w\to3$. We will refer to Eq. (10) as the reduced system of decoupled equations. In addition to the total energy and helicity, this system (valid for the resonant interactions that are assumed to be present in the small Ro regime) conserves a new set of quantities.

III. INVARIANT QUANTITIES AND STATISTICAL EQUILIBRIUM OF THE SMALL Ro REGIME

The systems of equations (9) and (10) conserve different sets of invariants. We use these differences to derive a statistical equilibrium for the strongly rotating turbulent flow limit (small Ro regime). Concerning the invariants, only quadratic quantities are considered below. In fact, spectrally truncated periodic representations of flows conserve only quadratic invariants. For example, full barotropic quasigeostrophic equations conserve energy and potential vorticity, but also an infinite number of invariants which are functions of the potential vorticity. The spectrally truncated periodic counterpart of the barotropic quasigeostrophic flow conserves only the first two quadratic invariants. The latter is not quadratic and is therefore not conserved by the periodic spectral truncation.

All calculations are carried out assuming a cylindrical spectrally truncated domain such that $k_h, |k_z| < k_T$, with k_T the truncation wavenumber. The discrete wavenumber increment is $\delta_\mathbf{k} = 2\pi/L$, where L^3 is the size of the domain occupied by the fluid.

A. Analysis of the full equations

Similarly to classical 3D Euler equations, rotating inviscid equations (9) conserve total energy (the helicity is also conserved, but we do not consider its effect on the analysis). Note that for nonrotating 3D turbulence, Kraichnan argued that the helicity did not change the forward cascade of energy to small scales, but could eventually delay such a cascade.[18]

Using Eq. (2), the total energy equation (6) can be rewritten as

$$E = \langle \mathbf{u}\mathbf{u}^* \rangle = \langle e(\mathbf{k}) \rangle = \sum_\mathbf{k} |a_+(\mathbf{k})|^2 + |a_-(\mathbf{k})|^2, \qquad (11)$$

where $\langle \cdot \rangle$ is the volume average and $k = |\mathbf{k}| = \sqrt{k_h^2 + k_z^2}$. Consider the phase space of $4N$ elements $(\Re[a_+(k_1)], \Im[a_+(k_1)], \Re[a_-(k_1)], \Im[a_-(k_1)],\ldots, \Im[a_-(k_N)])$, where N is the number of Fourier modes. The most probable probability density function in the phase space, or *Gibbs canonical distribution*, is

$$P_\alpha = C \exp(-\alpha E) = C \exp - \alpha \left[\sum_\mathbf{k} |a_+(\mathbf{k})|^2 + |a_-(\mathbf{k})|^2 \right], \qquad (12)$$

where C is the normalization constant of P_α such that $\int_{4N} P_\alpha = 1$, giving

$$\begin{aligned} C^{-1} &= \int_{\mathbb{R}^{4N}} \exp\left[-\alpha \sum_\mathbf{k} |a_+(\mathbf{k})|^2 + |a_-(\mathbf{k})|^2 \right] \\ &\quad \times d^N \Re(a_+) d^N \Im(a_+) d^N \Re(a_-) d^N \Im(a_-) \\ &= \left[\frac{1}{2}\sqrt{\frac{\pi}{\alpha}} \right]^{4N}, \end{aligned} \qquad (13)$$

where α is the Lagrange multiplier determined by the ensemble averaged energy. The classical result for the mean energy spectra can be recovered

$$\langle e(\mathbf{k}) \rangle_P = \langle |a_+(\mathbf{k})|^2 + |a_-(\mathbf{k})|^2 \rangle_P = \frac{2}{\alpha}, \qquad (14)$$

with $\alpha \neq 0$ and $\langle \cdot \rangle_P$ being the ensemble average calculated using P_α.

We consider the limit of large L to carry out the calculations using the integrals in the spectral domain of cylindrical truncation considered. We introduce the horizontal and vertical spectra, $E_h(k_h)$ and $E_z(k_z)$,

$$E = \int_0^{k_T} \int_{-k_T}^{k_T} \int_0^{2\pi} e(\mathbf{k}) d\mathbf{k} \qquad (15)$$

$$= \int_0^{k_T} E_h(k_h) dk_h \qquad (16)$$

$$= \int_{-k_T}^{k_T} E_z(k_z) dk_z. \qquad (17)$$

Equations (14)–(17) lead to the horizontal and vertical mean equipartiton energy spectra,

$$\langle E_h(k_h) \rangle_P = \frac{8\pi k_T}{\alpha} k_h, \quad \langle E_z(k_z) \rangle_P = \frac{2\pi k_T^2}{\alpha}. \qquad (18)$$

α can then be obtained from the total initial energy that is conserved and known, E_0, ($E_0 = \langle E \rangle = \langle E \rangle_P$) using

$$\alpha = \frac{4\pi k_T^3}{E_0}. \qquad (19)$$

In the weakly rotating limit, the flow is considered to be like classical isotropic nonrotating turbulence. It would thus be expected to relax to equipartition equation (18).[35] This

relaxation was, in fact, observed to be delayed by rotation in the simulations of inviscid weakly rotating flows. In addition, the large scales of the total isotropic spectrum were observed not to reach the equilibrium for some of the initial conditions (ICs).[36]

When focusing on the strongly rotating limit, we argue that the effects of the timescale separation and the much slower nonlinear timescale τ_1 discussed in Sec. II B must be incorporated into this analysis. In the next section, we examine the statistical equilibrium of this limit.

B. Analysis of the decoupled reduced equations

In the strong rotation limit, Eq. (10) has a new set of possible invariants (in addition to the total energy E). The quantities, elements of the set $S = (E_{3D}, E_{2D}, V_{2D}, E_w)$, are conserved by Eq. (10), where V_{2D} is the 2D enstrophy, defined by

$$V_{2D} = \frac{1}{2} \sum_{\mathbf{k} \in V_{\mathbf{k}}} |\omega_z(\mathbf{k})|^2, \tag{20}$$

and ω_z is the vertical component of the vorticity in spectral space.

The quantities in S are new constraints on the system's dynamics. Taking them into account gives a new expression for the probability density function,

$$P_{\alpha_1,\alpha_2,\alpha_3,\alpha_4} = C' \exp(-\alpha_1 E_{3D} - \alpha_2 E_{2D} - \alpha_3 V_{2D} - \alpha_4 E_w), \tag{21}$$

where C' is the normalization constant.

Considering the normal mode decomposition introduced in Sec. II A to be valid for all modes $\mathbf{k}$ such that $k_h \neq 0$, we can express the set of quantities S as follows using the same phase space variables introduced in Sec. III A. The use of the normal mode decomposition for all the modes leads to the generation of nonquadratic terms. We thus restrict the use of the helical normal mode decomposition to the nonzero frequency modes $\mathbf{k} \in W_{\mathbf{k}}$ such that both conditions $k_z \neq 0$ and $k_h \neq 0$ are imposed. For the modes in $V_{\mathbf{k}}$ we have

$$|\tilde{a}_+(\mathbf{k})|^2 + |\tilde{a}_-(\mathbf{k})|^2 - [\tilde{a}_+ \tilde{a}_-^*(\mathbf{k}) + \tilde{a}_+^* \tilde{a}_-(\mathbf{k})]$$
$$= |\mathbf{u}_{2D}(\mathbf{k})|^2 \quad \text{for } \mathbf{k} \in V_{\mathbf{k}}, \tag{22}$$

$$|\tilde{a}_+(\mathbf{k})|^2 + |\tilde{a}_-(\mathbf{k})|^2 + [\tilde{a}_+ \tilde{a}_-^*(\mathbf{k}) + \tilde{a}_+^* \tilde{a}_-(\mathbf{k})]$$
$$= |w(\mathbf{k})|^2 \quad \text{for } \mathbf{k} \in V_{\mathbf{k}}, \tag{23}$$

implying that

$$|\tilde{a}_+(\mathbf{k})|^2 + |\tilde{a}_-(\mathbf{k})|^2 = \tfrac{1}{2}(|\mathbf{u}_{2D}(\mathbf{k})|^2 + |w(\mathbf{k})|^2) \quad \text{for } \mathbf{k} \in V_{\mathbf{k}}. \tag{24}$$

The phase space can be re-expressed as the space of $4N$ modes,

$$\{\mathfrak{R}[a_+(k_1)], \mathfrak{I}[a_+(k_1)], \quad \mathfrak{R}[a_-(k_1)], \mathfrak{I}[a_-(k_1)], \ldots, \mathfrak{I}[a_-(k_M)],$$
$$\times \mathfrak{R}[u_{2D}(k_{M+1})], \mathfrak{I}[u_{2D}(k_{M+1})], \mathfrak{R}[w(k_{M+1})],$$
$$\times \mathfrak{I}[w(k_{M+1})], \ldots, \mathfrak{I}[w(k_N)]\},$$

with N number of Fourier modes and the last $N-M$ wave-

numbers, $k_{i \in [M+1,N]}$, being those satisfying $\mathbf{k} \in V_{\mathbf{k}}$, where $i \in \mathbb{N}$. Using the probability density functions (21) and (24) we can rewrite the probability density function as

$$P_{\alpha_1,\alpha_2,\alpha_3,\alpha_4} = C' \exp\left[-\alpha_1 \sum_{k_1}^{k_M} ([\mathfrak{R}(a_+)]^2 + [\mathfrak{R}(a_-)]^2 \right.$$
$$+ [\mathfrak{I}(a_+)]^2 + [\mathfrak{I}(a_-)]^2) - \sum_{k_{M+1}}^{k_N} (\alpha_2 + \alpha_3 k_h^2)$$
$$\times ([\mathfrak{R}(\mathbf{u}_{2D})]^2 + [\mathfrak{I}(\mathbf{u}_{2D})]^2)$$
$$\left. - \alpha_4 \sum_{k_{M+1}}^{k_N} ([\mathfrak{R}(w)]^2 + [\mathfrak{I}(w)]^2) \right]. \tag{25}$$

We obtain the ensemble averaged equilibrium spectra using Eq. (25),

$$\langle E_{3D}(k_h) \rangle_{P_{\alpha_1,\alpha_2,\alpha_3,\alpha_4}} = \frac{8\pi k_T}{\alpha_1} k_h,$$

$$\langle E_{3D}(k_z) \rangle_{P_{\alpha_1,\alpha_2,\alpha_3,\alpha_4}} = \frac{2\pi k_T^2}{\alpha_1}, \tag{26}$$

$$\langle E_{2D}(k_h) \rangle_{P_{\alpha_1,\alpha_2,\alpha_3,\alpha_4}} = \frac{2\pi k_h}{\alpha_2 + \alpha_3 k_h^2}, \tag{27}$$

$$\langle V_{2D}(k_h) \rangle_{P_{\alpha_1,\alpha_2,\alpha_3,\alpha_4}} = \frac{2\pi k_h^2}{\alpha_2 + \alpha_3 k_h^2}, \tag{28}$$

$$\langle E_w(k_h) \rangle_{P_{\alpha_1,\alpha_2,\alpha_3,\alpha_4}} = \frac{2\pi}{\alpha_4} k_h. \tag{29}$$

We can then estimate the four Lagrange multipliers using the values of $(E_{3D}, E_{2D}, V_{2D},$ and $E_w)$. This leads to

$$\alpha_1 = \frac{4\pi k_T^3}{E_{3D}}, \tag{30}$$

$$E_{2D} = \frac{\pi}{\alpha_3} \ln \left| 1 + \frac{\alpha_3}{\alpha_2} k_T^2 \right|, \tag{31}$$

$$V_{2D} = \pi \left[\frac{k_T^2}{\alpha_3} - \frac{\alpha_2}{\alpha_3^2} \ln \left| 1 + \frac{\alpha_3}{\alpha_2} k_T^2 \right| \right], \tag{32}$$

$$\alpha_4 = \frac{\pi k_T^2}{E_w}. \tag{33}$$

The constants α_2 and α_3 are solutions of the coupled system (31) and (32). They are obtained numerically starting from a first analytical estimation, valid when $(\alpha_3/\alpha_2)(V_{2D}/E_{2D}) \gg 1$,

$$\alpha_3 \approx \frac{\pi k_T^2/V_{2D}}{1 + \dfrac{E_{2D}}{V_{2D}} \dfrac{k_T^2}{\left(\exp\left[k_T^2 \dfrac{E_{2D}}{V_{2D}} \right] - 1 \right)}}, \tag{34}$$

$$\alpha_2 = \frac{\pi k_T^2}{E_{2D}} - \frac{\alpha_3 V_{2D}}{E_{2D}}. \tag{35}$$

IV. COMPARISON WITH NUMERICAL SOLUTIONS

We now compare the results we derived in Sec. III B to the numerical solutions that we obtained from solving Eq. (1).

We choose to focus on the homogeneous inviscid solutions in a finite domain. Both studies in finite and infinite domains are idealizations of rotating flows. Both approaches have advantages and limitations to direct applications. Here we use direct numerical simulation in a periodic domain to solve the Euler equations. The difficulty arises when the integral scales of the $W_{\mathbf{k}}$ and $V_{\mathbf{k}}$ modes grow and fill a large part of the domain, as the solutions become more dependent on the specific geometry of the domain of study.

Equation (1) is solved numerically using a direct (dealiased) pseudospectral method with a resolution 90.[3] A high resolution is not needed to obtain the statistical equilibrium of this truncated system. The integration domain is triply periodic of length 2π. We use the leapfrog time differencing and the Asselin–Robert filter to control the computational mode.[37] This leads to a nonexact conservation of the high frequency modes. In fact, the filter preferentially damps high frequency $W_{\mathbf{k}}$ modes in order to guarantee the stability of the computational mode of the leapfrog time-integration scheme. The "two-thirds rule" was chosen for dealiasing.

One set of simulations is initialized isotropically while the ICs of the second set are anisotropic, for which most of the energy is contained in the zero-frequency modes $V_{\mathbf{k}}$. With these choices we were able to investigate the tendencies of the system as it approaches its equilibrium state for various rotating rates. A range of rotation rates and the resulting inviscid spectra are compared to the results derived above.

The initial spectra are shown in Fig. 1. The set I of isotropic ICs, denoted IC: I, is initiated with the energy spectrum,

$$E(k) = A \exp[(k-8)/0.5]^2, \tag{36}$$

where $k = \sqrt{k_h^2 + k_z^2}$ is the isotropic wavenumber. Most of the energy is thus contained in the wave modes $W_{\mathbf{k}}$. The initial energy is peaked around $k_h = 8$ and $k_z = 7$. The constant A is chosen to give a total energy of $E = 0.1$.

The set II of ICs, denoted IC: II, is initiated with

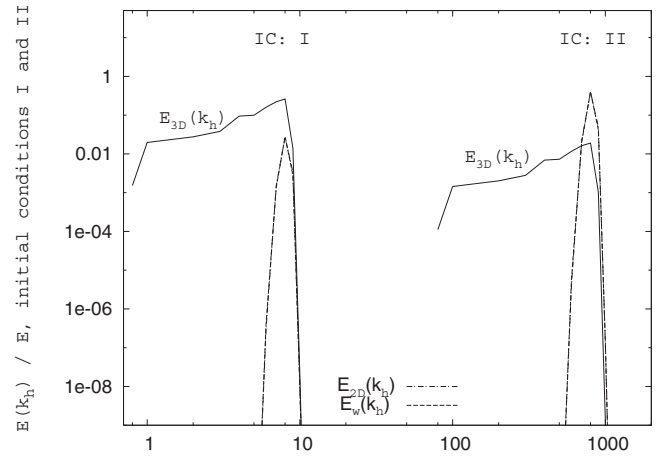$$E_{3D}(\mathbf{k} \in W_{\mathbf{k}}) = 0.0005B \exp[(k-8)/0.5]^2$$

and

FIG. 1. Initial horizontal spectra of ICs, IC: I and IC: II.

$$E(\mathbf{k} \in V_{\mathbf{k}}) = (E_{2D} + E_w)(\mathbf{k} \in V_{\mathbf{k}})$$
$$= 0.0995B \exp[(k-8)/0.5]^2. \tag{37}$$

B is a normalization constant set so that $E = 0.1$. Most of the initial energy in this configuration is contained in the zero-frequency modes $V_{\mathbf{k}}$.

A range of rotation rates was investigated. We only selected to display three key values of Ro. These values are similar to those identified in previous decay simulations.[13] The Rossby numbers were computed as

$$Ro = \frac{\sqrt{\langle \omega_z^2 \rangle}}{f} \tag{38}$$

and

$$Ro_{2D} = \frac{\sqrt{\langle \bar{\omega}_z^2 \rangle}}{f},$$

where $\bar{\omega}_z$ is the vertically averaged vertical component of the vorticity field corresponding to 2D $V_{\mathbf{k}}$ Fourier modes (with $k_z = 0$). Ro_{2D} gives a Rossby number specifically for the 2D modes.

The summary of the relevant parameters is displayed in Table I. The simulations with Ro = 0.01 initiated with both IC: I and IC: II were particularly difficult to run numerically. Their completion time was about 20 days of CPU time on an AMD Opteron 250, 2390 MHz.

A. Conservation and timescale

Figure 2 shows the time series of E_{2D} and E_{3D} for three values of Ro = 0.01, 0.2, and ∞ and up to dimensional time $\tilde{t} = 100$. The simulations initiated with close-to-isotropic conditions, IC: I, are displayed in Fig. 2(a). The simulations initiated with most of the energy containing modes in $V_{\mathbf{k}}$ are displayed in Fig. 2(b). Figure 3 shows the time series of V_{2D} and E_w for three values of Ro = 0.01, 0.2, and ∞. The timeseries are displayed up to the dimensional time $\tilde{t} = 100$ for both IC: I and IC: II.

The nonrotating simulations Ro $\rightarrow \infty$ initiated with both ICs, IC: I and IC: II, rapidly relax to a state of equilibrium. This equilibrium corresponds to the classical equipartition of

TABLE I. The timestep Δt, the rotation rate $f=2\Omega$, the final output time t_e, the 2D Rossby number Ro_{2D}, and the Robert filter parameter ρ for each of the selected simulations.

	IC: I					IC: II				
	Δt	f	t_e	Ro_{2D}	ρ	Δt	f	t_e	Ro_{2D}	ρ
Ro=0.01	2×10^{-4}	206.3	800	0.003	1×10^{-4}	2×10^{-4}	251.7	800	0.01	1×10^{-4}
Ro=0.2	2×10^{-4}	10.3	100	0.062	8×10^{-4}	2×10^{-4}	12.6	100	0.2	8×10^{-4}
Ro→∞	1×10^{-3}	0	100	∞	8×10^{-4}	1×10^{-3}	0	100	∞	8×10^{-4}

isotropic turbulence (not shown). The equipartitioned equilibrium of this simulation corresponds to the equipartitioned spectrum of conserved total energy equation (18). In terms of the modal decomposition equation (5), the breakdown of the isotropic equipartition reads $E_{3D}=0.098$ and $E_{2D}=0.001$, $E_w=0.001$, and for the enstrophy $V_{2D}=0.7$.

For both ICs, IC: I and IC: II, the Ro=0.2 solution approaches the values of the isotropic nonrotating equilibrium,

When initiated with IC: I, the Ro=0.2 solutions show an initial increase in E_{2D} and V_{2D}, which reach a maximum at $\tilde{t}=4$. This corresponds to the nondimensional time $t=40.2$, after which E_{2D} decreases and approaches the inviscid

system's equilibrium. This increase is surprising given that the equilibrium value of E_{2D} is actually lower than the initial value of E_{2D}. A mechanism of transfer from $W_{\mathbf{k}}$ to 2D modes is inducing this increase. This is reminiscent of the range of rotation identified in Bourouiba and Bartello, denoted the intermediate Ro range. The mechanism responsible for this increase could be attributed to near-resonant interactions since the timescale at which these interactions would be effective would correspond to $t\sim O(1/Ro^2)=25$ (Ref. 32) (dimensional time $\tilde{t}=2.42$). However, a smaller steady growth of the 2D energy is observable earlier in the simulation and occurs on a short timescale comparable to the linear time-
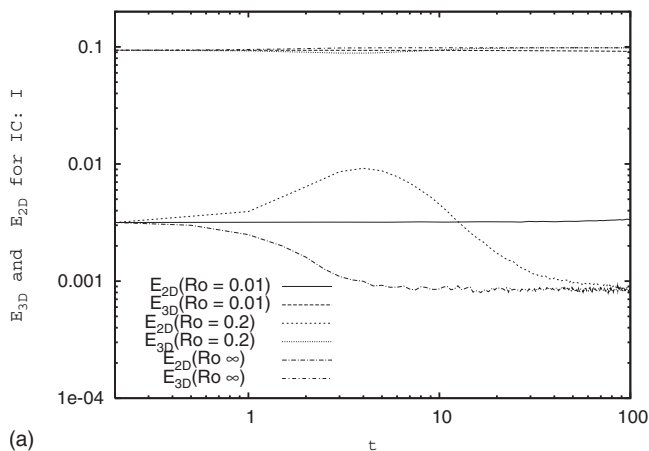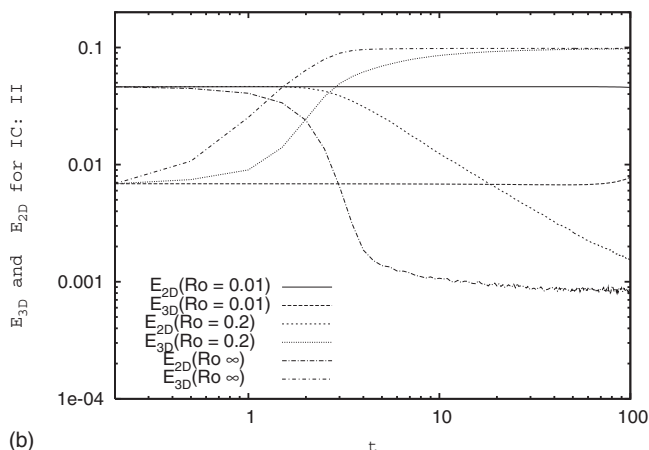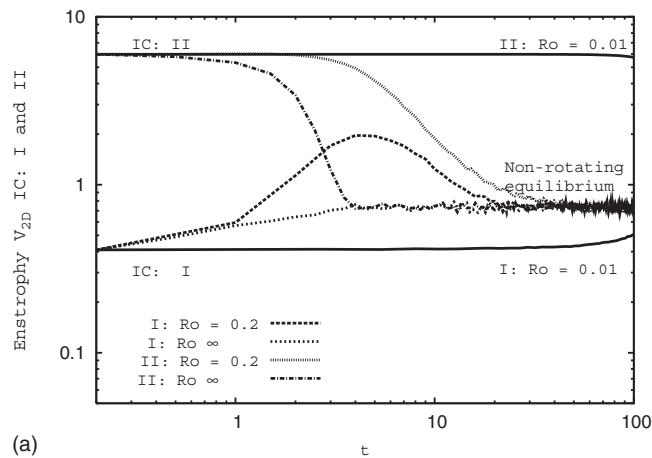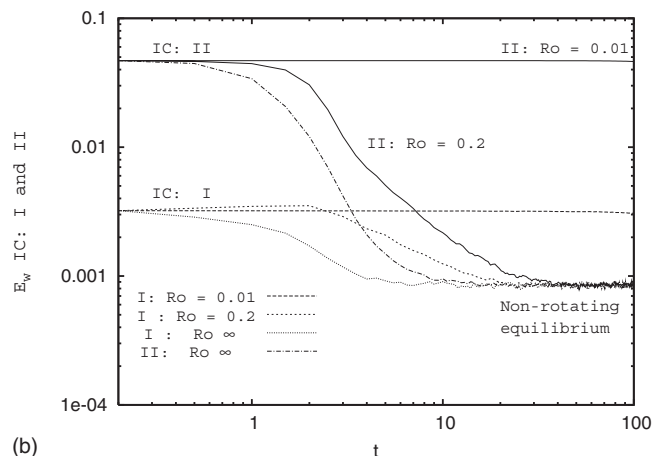

FIG. 2. Time series of the energy contributions E_{3D} and E_{2D} for Ro=∞, 0.2, and 0.01, initiated with IC: I (a) and IC: II (b). The time axis is the dimensional time.

FIG. 3. Time series of the 2D enstrophy V_{2D} (a) and the energy of the vertical component of the 2D field E_w (b) for Ro=∞, 0.2, and 0.01 for both IC: I and IC: II. The time axis is the dimensional time.

scale of the order $\tilde{t}=1/f=0.097$ [Ro=0.2 curve on Fig. 2(a)]. The mechanisms involved in the growth of 2D energy in this regime are still not well understood, but this is beyond the scope of the present study. Note that the increase in E_{2D} is not observable when starting with nearly 2D ICs, IC: II [Ro=0.2 curve on Fig. 2(b)]. Another mechanism is acting in this configuration, which is likely related to the destabilization of 2D structures and isotropization of 2D flows. The difference between IC: I and IC: II for the Ro=0.2 simulations suggests a dependence of the mechanism favoring the energy transfer from 3D to 2D modes on the initial distribution of energy between $W_{\mathbf{k}}$ and $V_{\mathbf{k}}$.

The focus of this study is the stronger rotation rate that corresponds to Ro=0.01. The Ro=0.01 simulations reveal a new set of quasi-invariants which is coherent with the set S of quantities conserved by the decoupled model (10). These are E_{2D} and E_{3D} in Fig. 2 and V_{2D} and E_w in Fig. 3. They are conserved when starting from both ICs (quasi-2D, IC: II, and quasi-isotropic 3D ICs, IC: I). However, Eq. (10) is valid at the first order of the asymptotic development only. We aim to quantify, using the simulations, the time to which the asymptotic expansion is valid and examine the behavior of the system at long times when the asymptotic development is no longer strictly valid. Thus, we extended the simulations of the smaller Ro started with both ICs (IC: I and IC: II) in order to investigate the timescale on which the invariants S are conserved.

Figure 4 shows the time series of the extended simulations of Ro=0.01 with IC: I and IC: II. Time has been rescaled to the nondimensional timescale $f\tilde{t}$. We can extract a relevant timescale at which the invariant regime is numerically valid. For both IC: I and IC: II, E_{3D} and E_{2D} are quasiconstant (E_{3D} is conserved at about 85% at the end of the simulations for both IC: I and IC: II due to the discriminating effect of the Robert filter) until a threshold time. This time is of the same order of magnitude for both sets of ICs, IC: I and IC: II, and is $t_\star \approx 20\,000$. This seems to confirm the asymptotic theories of decoupling predicting that the decoupling is valid until a time of the order $t_{\star,\text{theory}} \sim O(1/\text{Ro}^2) \approx 1 \times 10^4$. Note that the increase in E_{2D} observed for IC: I, Ro=0.01 is weak. This is consistent with the fact that the mechanism(s) responsible for the initial increase in 2D energy for IC: I, Ro=0.2 is specific to the intermediate Ro range.

In this section, we identified the time range on which the new set of invariants S critical for Eq. (21) are observable numerically. For $t<t_\star$, the quantities S are constant and the theoretical spectra derived are constant. For $t>t_\star$, the quantities S are now varying, so one would expect the theoretical spectra based on the existence of the invariants S to no longer be valid. The two questions addressed in the subsequent sections are: how do the theoretical spectra [Eqs. (26)–(29)] compare to those of the numerical solutions on the time range of conservation of S ($t<t_\star$), and how do the theoretical spectra compare to the simulation results beyond this time range ($t>t_\star$)?
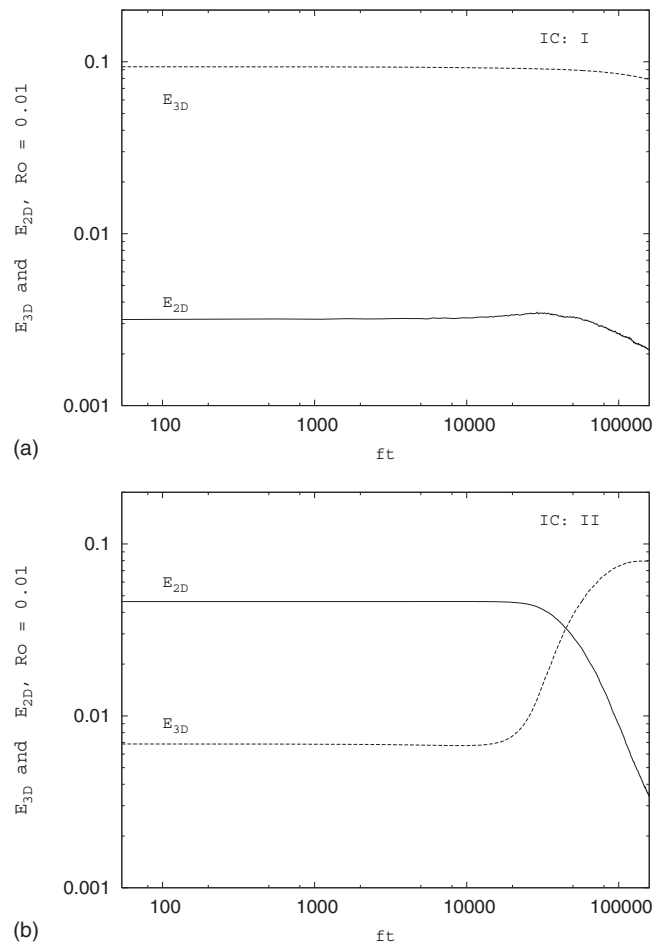

FIG. 4. Time series of the E_{2D} and E_{3D} for the Ro=0.01 simulation initialized with IC: I (a) and IC: II (b). The time axis is the nondimensional time $f\tilde{t}$.

B. Horizontal dynamics

We first focus on the horizontal dynamics. The time evolution of the spectra $E_{2D}(k_h)$, $E_w(k_h)$, and $E_{3D}(k_h)$ for both $t<t_\star$, for which the asymptotic first order decoupling is observed to hold, and $t>t_\star$, for which it is not, are displayed in Figs. 5 and 7. The horizontal spectra $E_{2D}(k_h)$, $E_w(k_h)$, and $E_{3D}(k_h)$ for simulations initiated with IC: I and IC: II are shown for $t \in [0\,ft_e]$. For $t<t_\star$, S are conserved and the decoupled description Sec. III B holds. This is the $V_{\mathbf{k}}$ decoupled phase. Hence, the theoretical spectra [Eqs. (26)–(29)] are constant, with those constants being calculated based on the invariants E_{2D}, E_{3D}, E_w, and V_{3D}. The numerical spectra agree with the theory: They quickly relax toward the predicted equilibrium spectra. In particular, for both ICs, the numerical spectra display the increase in energy in 2D horizontal large scales consistent with the theoretical predicted spectra, as shown in Fig. 5. The horizontal wavenumber characteristic of the 2D energy spectrum is defined as

$$\kappa_{h2D}(t) = \frac{\int_{\mathbf{k} \in V_{\mathbf{k}}} k_h E_{2D}(k_h,t) dk_h}{\int_{\mathbf{k} \in V_{\mathbf{k}}} E_{2D}(k_h,t) dk_h}. \tag{39}$$

It is used to indicate the direction of the transfer of the energy in classical 2D turbulence, and it is also called the cen-
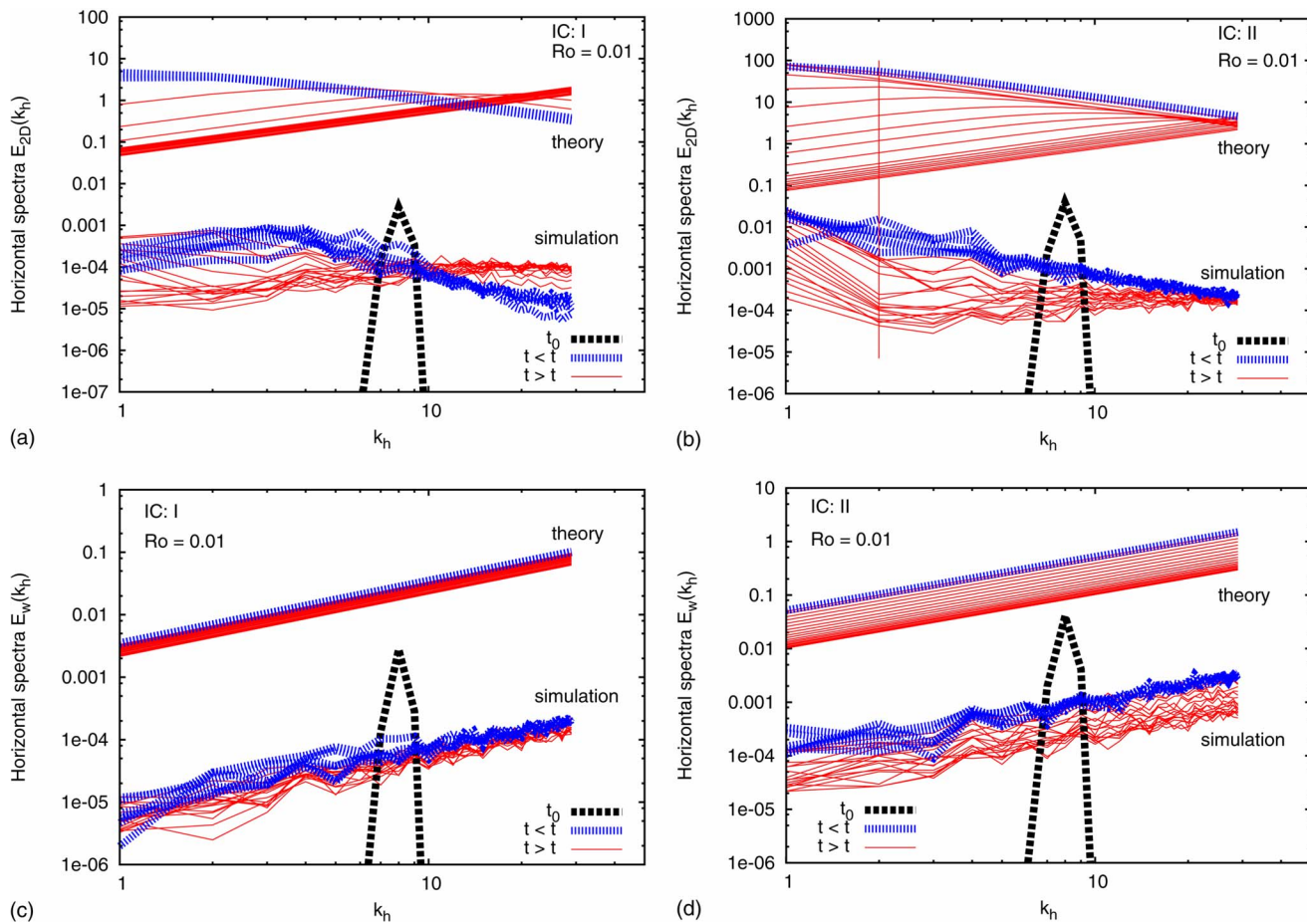
FIG. 5. (Color online) Horizontal wavenumber spectra of E_{2D} (upper panel) and E_w (lower panel) for Ro=0.01 and for IC: I (left column) and IC: II (right column). The theoretical spectra have been offset for clarity. The initial numerical spectra are denoted t_0 and multiple lines are for different times.

troid. We display the time evolution of the centroid, κ_{h2D}, for both IC: I and IC: II in Fig. 6. The centroid of 2D energy for the simulations initiated with IC: I starts decreasing after initially staying constant. It decreases until $t \approx t_\star$. The decrease in κ_{h2D} corresponds to an upscale transfer of E_{2D} similar to that observed in classical 2D turbulence. When
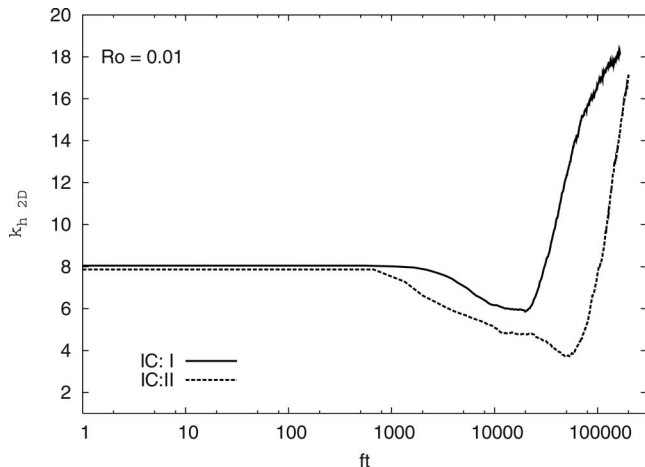

FIG. 6. Time series of κ_{h2D} [centroid of 2D energy spectra defined by Eq. (39)], with nondimensional time $f\bar{t}$ and for Ro=0.01. Both simulations started with IC: I and IC: II are shown.

starting with IC: II, the centroid of energy shows a similar dynamics and reaches a plateau at $t \approx t_\star$. However, it starts decreasing again for times $t_\star < t < 5 \times 10^4$, while the total E_{2D} is no longer invariant as in Fig. 4(a).

Figure 5 shows that during the decoupled phase $t < t_\star$ and for both IC: I and IC: II the $E_w(k_h)$ theoretical and numerical spectra are in good agreement. They show a horizontal forward cascade of the w energy, consistent with the passive scalar dynamics predicted by Eq. (10).

For $t > t_\star$, quantities S are no longer invariants. We consider the instantaneous values of the quantities S—now varying in time—to calculate the theoretical spectra [Eq. (26)–(29)]. At each time, instantaneous theoretical spectra are obtained. The reversal in the slope of $E_{2D}(k_h)$ showing a return to a downscale cascade is captured for both IC: I and IC: II. However, the larger horizontal 2D scales $k_h=1$ for the IC: II simulations retain more 2D energy compared to the theoretical prediction. For this time period, κ_{h2D} increases, which shows a reversal of dynamics and confirms the downscale 2D energy transfer (Fig. 6). For $t > t_\star$, $E_w(k_h)$ has similar dynamics to that of the decoupled phase. It corresponds to a forward horizontal energy transfer and an instantaneous equilibrium of equipartition of E_w among w modes.

Finally, concerning $E_{3D}(k_h)$, Fig. 7 shows that the theoretical equilibrium horizontal spectra initiated with IC: I vary
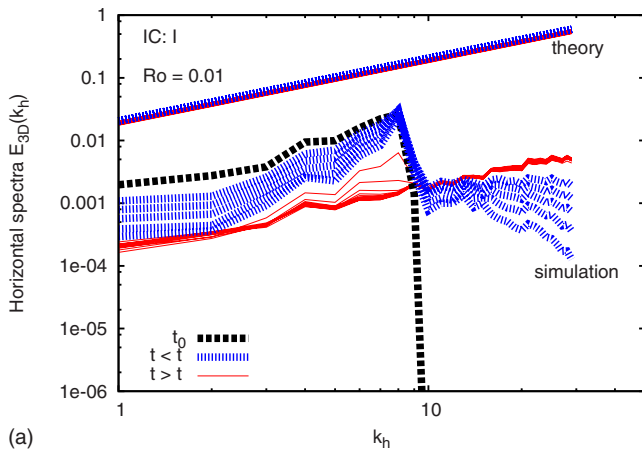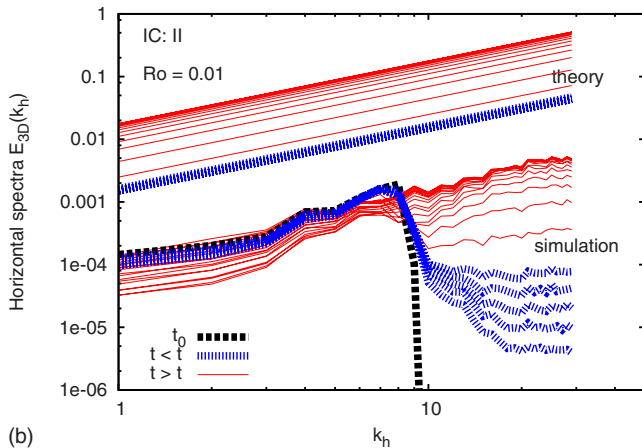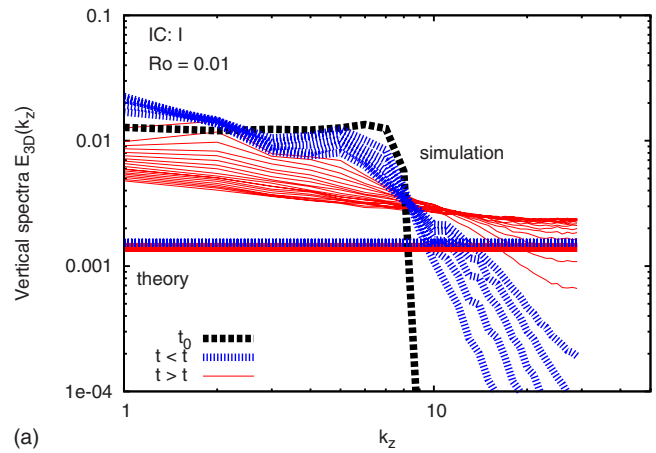
FIG. 7. (Color online) Horizontal wavenumber spectra E_{3D} for Ro=0.01 and for IC: I (a) and IC: II (b). The theoretical spectra have been offset for clarity. The initial numerical spectra are denoted t_0 and the multiple lines are for different times.

FIG. 8. (Color online) Vertical spectra of W_k 3D energy, $E_{3D}(k_z)$, for Ro=0.01 simulations initiated with IC: I (a) and IC: II (b). The initial numerical spectra are denoted t_0 and the multiple lines are for different times. The theoretical spectra have been offset for clarity only for the simulation IC: II (a).

very little in time. The larger 3D horizontal scales appear to lose energy in favor of the smaller horizontal 3D scales. When starting farther from the equipartition equilibrium [IC: II on Fig. 7(b)], the theoretical spectra keep the same slope, but increase in amplitude as E_{3D} increases. The numerical spectra show a tendency of $E_{3D}(k_h)$ to relax toward the theoretical equilibrium for both ICs.
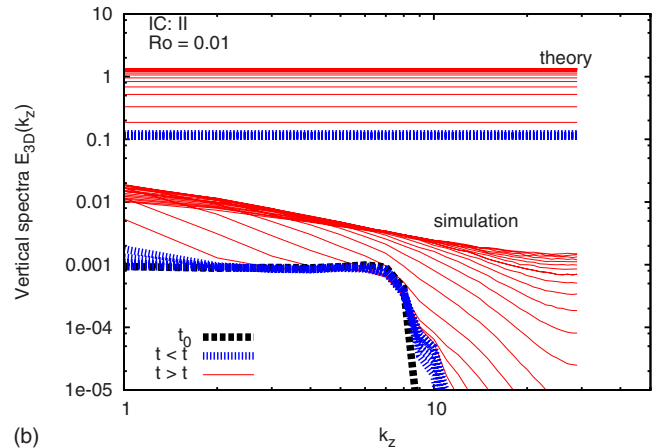
The equilibrium statistical mechanics captures the horizontal dynamical tendencies of the V_k and W_k modes accurately for both time windows $t < t_\star$ (strict validity of the decoupled model) and $t > t_\star$ (set of quantities S vary in time). Thus, when the set of quantities S is varying in time ($t > t_\star$), their variation is slow enough to allow the subsystem of V_k modes to relax to "instantaneous equilibrium" spectra on a short timescale. The horizontal dynamics of the W_k modes for IC: II suggests that the large scale 2D modes are losing energy in favor of the small horizontal scales of W_k modes.

C. Vertical dynamics and anisotropy

In Fig. 8, the vertical spectra of the W_k modes, $E_{3D}(k_z)$, are displayed for both ICs, IC: I and IC: II. The vertical equipartition of energy is not reached even at the end of the simulation for both initial conditions. When starting with a near-isotropy IC, IC: I, the 3D energy increases in the smaller k_z modes. This shows a transfer of 3D energy to larger vertical scales. Beyond $t_\star$ when the quantities S are determining the instantaneous horizontal short-time spectral equilibrium, the vertical dynamics of W_k seems very different. In both IC: I and IC: II, the vertical downscale transfers are weaker than what is expected by the equipartition equation (26) for both the $t < t_\star$ and $t > t_\star$ time windows.

Figure 9 shows the 3D energy density spectrum $e_{3D}(k_h, k_z)$ defined by

$$e_{3D}(k_h, k_z) = \frac{|\mathbf{u}_{3D}(k_h, k_z)|^2}{\text{Mo}(k_h, k_z)}, \qquad (40)$$

where $\text{Mo}(k_h, k_z)$ is the number of modes such that $k_h - 1/2 < k_h' < k_h + 1/2$ and $|k_z| - 1/2 < |k_z'| < |k_z| + 1/2$. This spectrum provides more information about the anisotropy noted above. Note that an equipartition of 3D energy corresponds to a flat $k_h - k_z$ spectrum. The initial isotropic distribution of energy corresponding to IC: I and IC: II is shown by a $e_{3D}(k_h, k_z, t_0)$ spectrum in the top panel of Fig. 9. Note that only the intensity of energy contained in the 3D modes changes from IC: I to IC: II [see Eqs. (36) and (37)], but the distribution of the energetic W_k modes does not change.
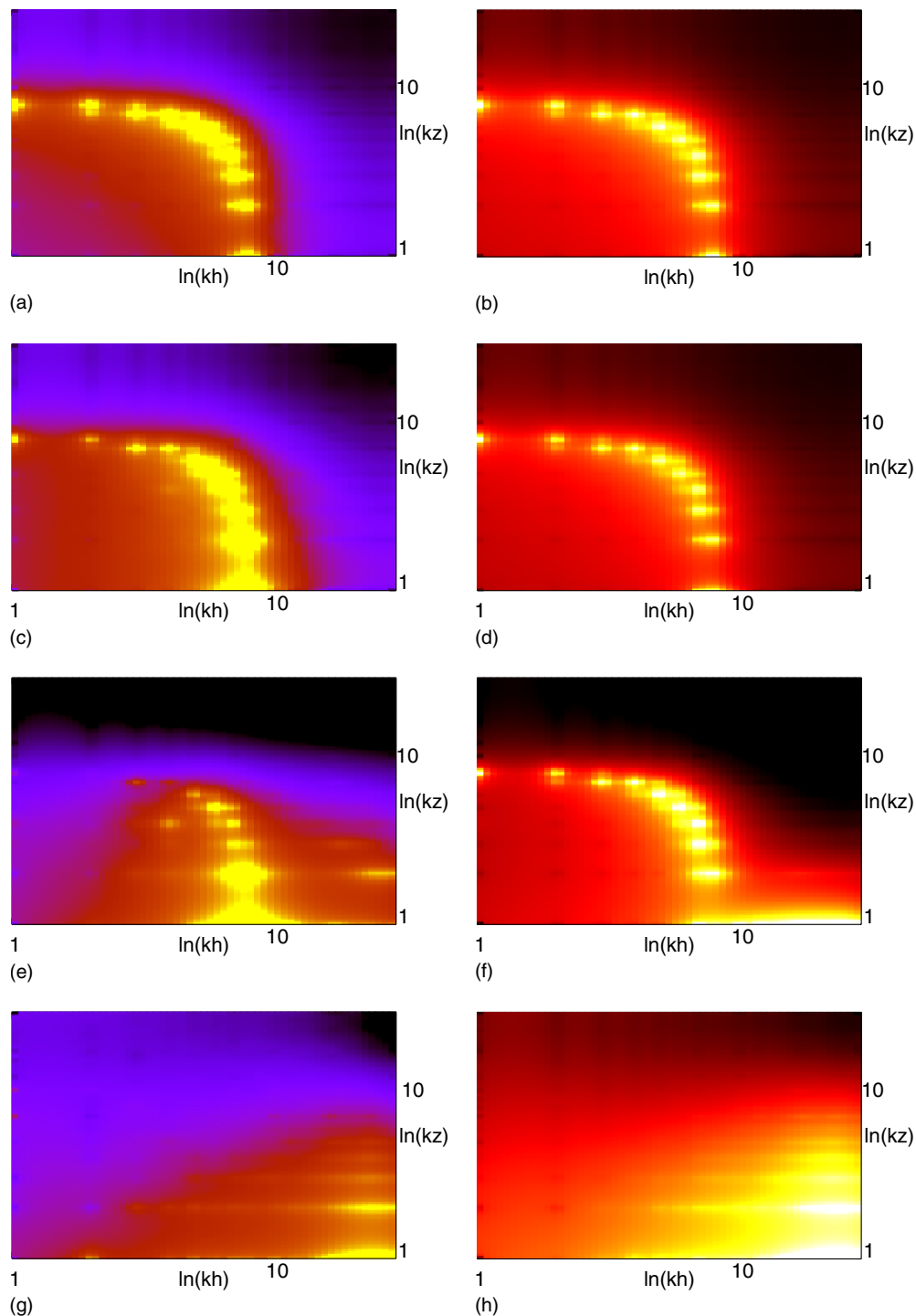
FIG. 9. (Color online) Time averaged 3D energy spectrum $e_{3D}(k_h, k_z)$ in log-log scale at an initial time t_0 [(a) and (b)], an intermediate time range below $t_\star$ such that $t_1 \in [460, 1.38 \times 10^4]$ [(c) and (d)], an intermediate time $t_2 \in [2.3 \times 10^4, 4.6 \times 10^4]$ [(e) and (f)], and the end of the simulations with $t_3 \in [1.6 \times 10^5, 1.8 \times 10^5]$ [(g) and (h)]. Both the t_2 and t_3 time ranges correspond to times larger than $t_\star$, i.e., beyond the decoupled phase. Ro=0.01 and the ICs are IC: I (left column) and IC: II (right column). The colors are normalized for each graph such that the maximum (minimum) value of the modal spectrum is represented by the brightest (darkest) color.

In the initial phase of decoupling ($t < t_\star$), the 3D energy spectrum does not vary for either IC. However, a slight preferential redistribution of energy occurs in favor of the energy-containing modes with smaller frequencies (small k_z/k), especially for IC: I (see region below the $k_h = k_z$ diagonal). This is not surprising given the tendency of the resonant $33 \rightarrow 3$ interactions to transfer 3D energy toward $W_\mathbf{k}$

modes of smaller frequency $\omega_\mathbf{k}$.[31] Recall that the resonant interactions in Eq. (10) are assumed to be predominant in the decoupled regime of time $t < t_\star$. Our observation is consistent with the theoretical analysis of Galtier in which an anisotropic decomposition of wave numbers in $k_h - k_z$ confirmed theoretically the tendency of the resonant interactions to develop and maintain anisotropy.

For $t > t_\star$, however, it is expected that nonresonant interactions are active. We can see in Fig. 9 that the apparent transfer of 3D energy to the larger vertical 3D scales (observable in the vertical spectra, see Fig. 8) still acts to preferentially concentrate energy in the large vertical scale (small k_z) and small horizontal scale (large k_h) $W_\mathbf{k}$ modes (lower right corner of the $k_h - k_z$ plane in Fig. 9). This is particularly true toward the end of both simulations IC: I and IC: II [Figs. 9(g) and 9(h)].

When looking at the set of quasi-2D ICs, IC: II, we note that the preferential region of transfer of energy from the $V_\mathbf{k}$ 2D modes to the $W_\mathbf{k}$ 3D modes is in favor of the small horizontal and large vertical scales. At the end of both IC: I and IC: II simulations the equipartition is not reached (here we are referring to the equipartition expected to be reached when Ro$\rightarrow \infty$, i.e., flat spectrum) and if the process of redistribution toward equipartition is occurring it seems to be much reduced by the effect of rotation, even in the coupled stage (involving interactions that are not resonant).

The vertical dynamics of the $W_\mathbf{k}$ wave modes suggest that the energy is preferentially transferred to the region of low frequency (large k_h and small k_z) modes, when a significant 3D energy is present initially (i.e., IC: I). When starting with a dominant 2D energy, the energy transfers from 2D to 3D modes are done locally frequency wise, leading to a transfer in favor of the low wave frequencies (large k_h and small k_z). This anisotropy in favor of the small frequency spectral region is very long lasting and coincides with an inhibition of the 3D energy transfers toward small vertical small horizontal scales (top right corner of the $k_h - k_z$ phase in Fig. 9) during both the decoupled and coupled stages ($t < t_\star$ and $t > t_\star$).

V. DISCUSSION

The main purpose of this study has been to examine the dynamics of the small Ro range. This is the third of three rotating ranges previously identified: weakly, intermediate, and strongly rotating.[13] In the small Ro limit several dynamics were discussed in the literature. On the one hand some theoretical results predict a decoupling of the wave from the zero-frequency modes. These results include the analysis of Babin et al.,[33,38] the studies of weakly resonant waves,[31] and the wave-turbulence approach used by Galtier (2003). However, note that theoretical results of the wave-turbulence approach are not valid in the small k_z and the large k_h spectral domain. On the other hand extended wave-turbulence results by Cambon et al.[34] suggested that such decoupling cannot be reached due to coupling terms remaining active even in the Ro$\rightarrow 0$ limit.

Our focus has been to investigate the inviscid dynamics of a strongly rotating spectrally truncated turbulent flow, starting with the analysis of the statistical equilibrium of a model of flow in which zero-frequency and wave modes are decoupled. Our tool of study was equilibrium statistical mechanics. For comparison, we also examined numerically the effect of rotation on the equilibrium of an inviscid unforced truncated rotating turbulent system for different ICs and for moderate to strong rotation rates.

We started by deriving the theoretical spectra for the decoupled wave and zero-frequency modes. This was complemented by a numerical study of the inviscid dynamics which showed two phases: a first decoupled phase for $t < t_\star$ and a coupled phase for $t > t_\star$. Thus, the prediction of decoupling of the wave and zero-frequency modes in the asymptotic limit of Ro$\rightarrow 0$ is valid and observable numerically. For both coupled and decoupled time phases, we find a reduction of the vertical energy transfers to small vertical scales.

During the decoupled time phase ($t < t_\star$) the new set of invariant characteristic of the theoretical model of decoupled equations is found to be in agreement with the numerical simulation of the full truncated inviscid equations. The time until which the decoupling is observable is found to be $t_\star \sim 2/\text{Ro}^2$, which is consistent with the weakly nonlinear resonant wave theory prediction. This evaluation is robust to the change of ICs from 2D to 3D initial flows. The theoretical spectra derived from statistical equilibrium assumptions captured the horizontal dynamics of the decoupled system accurately. We observed an upscale horizontal transfer of the 2D energy and a forward horizontal transfer of 3D and w energies. This dynamics is in agreement with the "global splitting" result by Babin et al., predicting a decoupling of the 2D and w modes from the 3D modes, an inverse cascade of 2D energy, a direct cascade of 3D energy, and a passive scalar dynamics for the w modes.

The equilibrium statistical mechanics spectra predicted a vertical equipartition of the 3D energy; however, we observe a preferential concentration of wave energy in the smaller frequency wave modes. This preferential concentration is not consistent with the vertical dynamics of the decoupled model of Babin et al.[38] In fact, they predict a "freezing" of the vertical 3D energy transfers. On the other hand, weak wave theories predict that triple inertial wave resonant interactions transfer energy to smaller frequency modes (excluding the zero-frequency modes).[31] The anisotropy was also found to be consistent with the spectral predictions of wave-turbulence kinetic energy equations built on the resonant inertial wave interactions.[39] The numerical results obtained by Bellet et al.[16] simulating inertial wave resonant interactions only between nonzero frequency modes showed a tendency of the 3D wave modes to concentrate the energy in the lower frequency modes. However, these wave-turbulence results are valid in a restricted spectral domain not including the zero-frequency modes. Hence, the advantage of the inviscid simulations presented here is that they confirm the development of anisotropy in the decoupled system of modes containing all the modes (both the zero-frequency and the 3D modes). Finally, another conserved quantity is necessary in order to improve the prediction of the decoupled vertical dynamics. Accounting for the influence of the conservation of the wave mode's helicity or the conservation of energy by triple resonant wave mode interactions could also help improve the wave equilibrium statistical mechanics spectra derived.

In the coupled phase ($t > t_\star$), the set of invariants corresponding to the decoupled equations is no longer conserved quantities. However, the simulations show that their variation

timescale is long enough to consider them quasi-invariants on the short timescale. The corresponding time-varying theoretical horizontal spectra are in agreement with the instantaneous numerical spectra, accurately capturing the instantaneous horizontal dynamics of the now-coupled wave and zero-frequency modes. Hence, the set of slowly varying "invariants" still plays a constraining role on the short-time dynamics. This is reminiscent of the example of the inviscid stratified truncated Boussinesq equations which have constraining quasi-invariants on the short-time dynamics of the slow modes.[28]

The large horizontal scales of the zero-frequency modes lose energy to the now coupled wave modes. After an initial upscale horizontal transfer taking place during the decoupled phase, the transfer of 2D energy starts to favor the 2D small horizontal scales. In this coupled phase, the vertical anisotropy observed in the decoupled phase persists. In fact, the wave energy remains predominantly contained in the large vertical and small horizontal scales.

Finally, in the coupled phase, an initially 3D flow led to a transient increase in 2D energy. The 2D energy reaches its statistical equilibrium after a phase of increase and then decrease with time. The initial growth is not observed for both ICs. When the IC is 2D, the growth is not observed, suggesting that the mechanism leading to the transient growth 2D energy depends on the initial ratio of energy between $W_{\mathbf{k}}$ and $V_{\mathbf{k}}$. The rate of this 2D energy increase varies with Ro. It is stronger for a flow with Ro≈ 0.2 compared to the flow with Ro$=0.01$. The energy transfer from 3D to 2D causing the increase in 2D energy is reminiscent of the intermediate Ro range identified in the decaying simulations of Bourouiba and Bartello. The mechanisms responsible for this increase could be attributed to near resonance. In fact, the forced simulations of Smith and Lee suggested that near-resonant interactions were responsible for the 3D to 2D transfers at the moderately small Ro that they examined. If that was the case, we would expect the timescale on which near-resonant interactions act to correspond to $t \sim O(1/\text{Ro}^2)$.[32] However, we observe that the steady growth of 2D energy occurs earlier in the Ro$=0.2$ simulation. It starts at a time comparable to the linear timescale of rotation of the order of $1/f$. This timescale suggests that the mechanism responsible for the transient 2D energy increase could also be initiated by linear effects. In fact, linear effects were proposed as an explanation to the increase in 2D energy in an inhomogeneous rotating flow.[15] Finally, much more understanding is needed to explain the mechanisms occurring beyond the decoupled phase $(t > t_\star)$. In the small Ro limit, where a clear coupling phase follows the decoupling phase, this mechanism remains weaker than that observed in the coupled phase of flows with larger Ro. What the present inviscid simulations suggest is a confirmation of the existence of the a mechanism depending nonmonotonically on Ro, inherent to the rotating flow dynamics in the coupled phase, and which is at the origin of the intermediate Ro regime observed in decaying rotating flows.[13]

APPENDIX: NORMAL MODES

The linearization of the rotating barotropic vorticity equations around a rest base state gives

$$\frac{\partial \omega}{\partial t} = (f\hat{\mathbf{z}} \cdot \nabla)\mathbf{u}, \tag{A1}$$

with $\omega = (\omega_x, \omega_y, \omega_z)$ the vorticity vector and $\mathbf{u} = (u, v, w)$ is the velocity vector. Its transformation to Fourier space leads to

$$\frac{\partial}{\partial t}\mathbf{W}_{\mathbf{k}} = M_{\mathbf{k}}\mathbf{W}_{\mathbf{k}}, \tag{A2}$$

with

$$\mathbf{W}_{\mathbf{k}} = \begin{pmatrix} \hat{\omega}_x \\ \hat{\omega}_y \\ \hat{\omega}_z \end{pmatrix},$$

$$M_{\mathbf{k}} = \begin{pmatrix} 0 & -ifk_z^2/k^2 & +ifk_zk_y/k^2 \\ +ifk_z^2/k^2 & 0 & -ik_zk_x/k^2 \\ -ifk_zk_y/k^2 & +ifk_zk_x/k^2 & 0 \end{pmatrix}, \tag{A3}$$

where

$$\begin{pmatrix} \omega_x \\ \omega_y \\ \omega_z \end{pmatrix}(x,y,z,t) = \Sigma_{\mathbf{k}} \begin{pmatrix} \hat{\omega}_x \\ \hat{\omega}_y \\ \hat{\omega}_z \end{pmatrix} \exp(i\mathbf{k} \cdot \mathbf{r}), \tag{A4}$$

with $\mathbf{r}$ being the position vector (x,y,z) and $i^2 = -1$. If we restrict ourselves to fluids in a periodic domain of size $L \times L \times L$, we have $\mathbf{k} = (k_x, k_y, k_z) = (m_x, m_y, m_z)2\pi/L$, with $(m_x, m_y, m_z) \in \mathbb{Z}^3$, the set of integers.

The diagonalization of this system leads to the eigenvalues

$$\lambda_s = sfk_z/k$$

and

$$\lambda_0 = 0, \tag{A5}$$

with $s = \pm$. The associated eigenvectors are

$$\mathbf{n}_{\lambda_s} = \mathbf{n}_s = \begin{pmatrix} -k_xk_z/k_h^2 + isk_yk/k_h^2 \\ -k_yk_z/k_h^2 - isk_xk/k_h^2 \\ 1 \end{pmatrix}, \quad \mathbf{n}_{\lambda_0} = \mathbf{k} = \begin{pmatrix} k_x \\ k_y \\ k_z \end{pmatrix}. \tag{A6}$$

The horizontal wavevector is $k_h = \sqrt{k_x^2 + k_y^2}$. The derivation of the eigenvectors requires that $k_z \neq 0$ and $k_h \neq 0$. From Eq. (A6) we see that $\mathbf{n}_s$ and $\mathbf{n}_{-s}$ are complex conjugates and that $(\mathbf{k}, \mathbf{n}_s, \mathbf{n}_{-s})$ forms an orthogonal basis, i.e., $\mathbf{n}_s^* = \mathbf{n}_{-s}$ and

$\mathbf{k} \cdot \mathbf{n}_s^* = \mathbf{k} \cdot \mathbf{n}_{-s}^* = \mathbf{n}_s \cdot \mathbf{n}_{-s}^* = 0$ (* is used for complex conjugate). It is easy from Eq. (A6) to show that $\mathbf{n}_s(-\mathbf{k}) = \mathbf{n}_{-s}(\mathbf{k})$ and that $|\mathbf{n}_s| = 2$.

Due to the continuity equation, $\nabla \cdot \mathbf{u} = 0$, the decomposition of the velocity field leads to components only on $(\mathbf{n}_+, \mathbf{n}_-)$, i.e., a zero component on $\mathbf{k}$.

This gives a decomposition of the implicitly nondivergent velocity field,

$$\mathbf{u}(\mathbf{r}) = \sum_{\mathbf{k}} \mathbf{u}(\mathbf{k}) \exp(i\mathbf{k} \cdot \mathbf{r})$$

$$= \sum_{\mathbf{k}} [A_+(\mathbf{k},t)\mathbf{n}_+(\mathbf{k}) + A_-(\mathbf{k},t)\mathbf{n}_-(\mathbf{k})] \exp(i\mathbf{k} \cdot \mathbf{r}),$$

(A7)

with $A_s(\mathbf{k},t) = a_s(\mathbf{k})\exp(i\lambda_s t)$. The reality condition $[\mathbf{u}(\mathbf{r})$ must be real] implies that $\mathbf{u}^*(\mathbf{k}) = \mathbf{u}(-\mathbf{k})$. Thus, the Fourier components $a_s(\mathbf{k})$ satisfy $a_s^*(\mathbf{k}) = a_s(-\mathbf{k})$.

The decomposition of the flow field into these *inertial waves*, Eq. (A7), corresponds to the *helical mode* decomposition.[1,40] Equivalent decompositions include the Craya–Herring decomposition[41,42] and the poloidal-toroidal decomposition.[16,40]

[1]H. P. Greenspan, *The Theory of Rotating Fluid* (Cambridge University Press, Cambridge, 1968).

[2]A. D. McEwan, "Inertial oscillations in a rotating fluid cylinder," J. Fluid Mech. **40**, 603 (1969).

[3]A. D. McEwan, "Angular momentum diffusion and the initiation of cyclones," Nature (London) **260**, 126 (1976).

[4]E. J. Hopfinger, K. F. Browand, and Y. Gagne, "Turbulence and waves in a rotating tank," J. Fluid Mech. **125**, 505 (1982).

[5]L. Jacquin, O. Leuchter, C. Cambon, and J. Mathieu, "Homogeneous turbulence in the presence of rotation," J. Fluid Mech. **220**, 1 (1990).

[6]C. Baroud, B. Plapp, Z.-S. She, and H. Swinney, "Anomalous self-similarity in a turbulent rapidly rotating fluid," Phys. Rev. Lett. **88**, 114501 (2002).

[7]C. Morize, F. Moisy, and M. Rabaud, "Decaying grid-generated turbulence in rotating tank," Phys. Fluids **17**, 095105 (2005).

[8]P. K. Yeung and Y. Zhou, "Numerical study of rotating turbulence with external forcing," Phys. Fluids **10**, 2895 (1998).

[9]L. M. Smith and F. Waleffe, "Transfer of energy to two-dimensional large scales in forced, rotating three-dimensional turbulence," Phys. Fluids **11**, 1608 (1999).

[10]Q. Chen, S. Chen, G. L. Eyink, and D. D. Holm, "Resonant interactions in rotating homogeneous three-dimensional turbulence," J. Fluid Mech. **542**, 139 (2005).

[11]J. Bardina, J. H. Ferziger, and R. S. Rogallo, "Effect of rotation on isotropic turbulence: computation and modelling," J. Fluid Mech. **154**, 321 (1985).

[12]P. Bartello, O. Métais, and M. Lesieur, "Coherent structures in rotating three-dimensional turbulence," J. Fluid Mech. **273**, 1 (1994).

[13]L. Bourouiba and P. Bartello, "The intermediate Rossby number range and 2d-3d transfers in rotating decaying homogeneous turbulence," J. Fluid Mech. **587**, 139 (2007).

[14]L. M. Smith and Y. Lee, "On near resonances and symmetry breaking in forced rotating flows at moderate Rossby number," J. Fluid Mech. **535**, 111 (2005).

[15]P. A. Davidson, P. J. Staplehurst, and S. B. Dalziel, "On the evolution of eddies in a rapidly rotating system," J. Fluid Mech. **557**, 135 (2006).

[16]F. Bellet, F. Godeferd, J. Scott, and C. Cambon, "Wave-turbulence in rapidly rotating flows," J. Fluid Mech. **23**, 81 (2006).

[17]R. H. Kraichnan, "Inertial ranges in two-dimensional turbulence," Phys. Fluids **10**, 1417 (1967).

[18]R. H. Kraichnan, "Helical turbulence and absolute equilibrium," J. Fluid Mech. **59**, 745 (1973).

[19]R. H. Kraichnan, "Statistical dynamics of two-dimensional flow," J. Fluid Mech. **67**, 155 (1975).

[20]G. Holloway, "Eddies, waves, circulation, and mixing: Statistical geofluid mechanics," Annu. Rev. Fluid Mech. **18**, 91 (1986).

[21]A. J. Majda and X. Wang, *Nonlinear Dynamics and Statistical Theories for Basic Geophysical Flow* (Cambridge University Press, Cambridge, 2006).

[22]D. G. Fox and S. A. Orszag, "Inviscid dynamics of two-dimensional turbulence," Phys. Fluids **16**, 169 (1972).

[23]R. Salmon, G. Holloway, and M. C. Hendershott, "The equilibrium statistical mechanics of simple quasi-geostrophic models," J. Fluid Mech. **75**, 691 (1976).

[24]R. V. Abramov and A. J. Majda, "Statistically relevant conserved quantities for truncated quasigeostrophic flow," Proc. Natl. Acad. Sci. U.S.A. **100**, 3841 (2003).

[25]T. Warn, "Statistical mechanical equilibria of the shallow water equations," Tellus, Ser. A **38A**, 1 (1986).

[26]P. Bartello, "Geostrophic adjustment and inverse cascades in rotating stratified turbulence," J. Atmos. Sci. **52**, 4410 (1995).

[27]Y. Kaneda, T. Gotoh, and N. Bekki, "Dynamics of inviscid truncated model of two-dimensional turbulent shear flow," Phys. Fluids A **1**, 1225 (1989).

[28]M. L. Waite and P. Bartello, "Stratified turbulence dominated by vortical motion," J. Fluid Mech. **517**, 281 (2004).

[29]C. Cichowlas, P. Bonaiti, F. Debbasch, and M. Brachet, "Effective dissipation and turbulence in spectrally truncated Euler flows," Phys. Rev. Lett. **95**, 264502 (2005).

[30]W. J. Bos and J.-P. Bertoglio, "Dynamics of spectrally truncated inviscid turbulence," Phys. Fluids **18**, 071701 (2006).

[31]F. Waleffe, "Inertial transfers in the helical decomposition," Phys. Fluids A **5**, 677 (1993).

[32]A. C. Newell, "Rossby wave packet interactions," J. Fluid Mech. **35**, 255 (1969).

[33]A. Babin, A. Mahalov, and B. Nicolaenko, "Global splitting, integrability and regularity of 3d Euler and Navier–Stokes equations for uniformly rotating fluids," Eur. J. Mech. B/Fluids **15**, 291 (1996).

[34]C. Cambon, R. Rubinstein, and F. S. Godeferd, "Advances in wave turbulence: Rapidly rotating flows," New J. Phys. **6**, 73 (2004).

[35]T. Lee, "On some statistical properties of hydrodynamical and magnetohydrodynamical fields," Q. Appl. Math. **10**, 69 (1952).

[36]Y. Yamazaki, Y. Kaneda, and R. Rubeinstein, "Dynamics of inviscid truncated model of rotating turbulence," J. Phys. Soc. Jpn. **71**, 81 (2002).

[37]R. Asselin, "Frequency filter for time integrations," Mon. Weather Rev. **100**, 487 (1972).

[38]A. Babin, A. Mahalov, and B. Nicolaenko, "On nonlinear baroclinic waves and adjustment of pancake dynamics," Theor. Comput. Fluid Dyn. **11**, 215 (1998).

[39]S. Galtier, "Weak inertial-wave turbulence theory," Phys. Rev. E **68**, 015301 (2003).

[40]F. Waleffe, "The nature of triad interactions in homogeneous turbulence," Phys. Fluids A **4**, 350 (1992).

[41]A. Craya, *Contribution à l'analyse de la turbulence associée à des vitesses moyennes*, P.S.T. Ministère de l'Air 34, 1958.

[42]J. R. Herring, "Approach of axisymmetric turbulence to isotropy," Phys. Fluids **17**, 859 (1974).